Near surface roughness estimation: a parameterization derived from artificial rainfall experiments and two-dimensional hydrodynamic modelling for multiple vegetation coverages

David Feldmann, Patrick Laux, Andreas Heckl, Manfred Schindler, Harald Kunstmann

Angaben zur Veröffentlichung / Publication details:

Feldmann, David, Patrick Laux, Andreas Heckl, Manfred Schindler, and Harald Kunstmann. 2023. "Near surface roughness estimation: a parameterization derived from artificial rainfall experiments and two-dimensional hydrodynamic modelling for multiple vegetation coverages." *Journal of Hydrology* 617 (Part A): 128786. https://doi.org/10.1016/j.jhydrol.2022.128786.

Journal of Hydrology 617 (2023) 128786

Contents lists available at ScienceDirect

Journal of Hydrology

journal homepage: www.elsevier.com/locate/jhydrol

Research papers

Near surface roughness estimation: A parameterization derived from artificial rainfall experiments and two-dimensional hydrodynamic modelling for multiple vegetation coverages

David Feldmann [a], Patrick Laux [a,b,*], Andreas Heckl [c], Manfred Schindler [c], Harald Kunstmann [a,b]

[a] Karlsruhe Institute of Technology, Campus Alpin, Kreuzeckbahnstraße 19, Garmisch-Partenkirchen, 82467, Germany
[b] University of Augsburg, Institute of Geography, Alter Postweg 118, Augsburg, 86159, Germany
[c] Dr. Blasy - Dr. Øverland Ingenieure GmbH, Moosstraße 3, Eching am Ammersee, 82275, Germany

ARTICLE INFO

This manuscript was handled by Marco Borga, Editor-in-Chief, with the assistance of Francesco Comiti, Associate Editor.

Keywords:
Depth-dependent roughness coefficients
Flow resistance
Artificial rainfall experiments
Hydraulic rainfall-runoff modelling
Surface runoff
Flash floods

ABSTRACT

Roughness is the key parameter for surface runoff simulations. This study aims to determine robust Manning resistance coefficients (n) on the basis of consecutive artificial rainfall experiments on natural hillslopes available in literature, obtained at 22 different sites with different degrees of vegetation cover and type. The Manning resistance coefficient is particularly important in the context of two-dimensional (2D) hydraulic heavy rainfall simulations. Since there is a wide range of possible resistance values available leading to significantly different results regarding the accumulation of surface runoff, especially for shallow water depths. The planning of flood protection structures is directly affected by these uncertainties. This work also improves the knowledge between roughness and the shape of the hydrograph allowing a better calibration of infiltration models. As flow velocity, water depth, and infiltration rate were not observed during the rainfall experiments, only the outflow of the test field and rain intensity are known. For this purpose, a framework was developed to parameterize shallow water depth (< 1 cm) -dependent roughness coefficients. To test the robustness of the framework, three different formulations of depth-dependent roughness and a constant Manning coefficient are used by comparing the measured discharge under different rainfall intensities with simulations in a 2D-hydraulic model. We identified a strong dependency of Manning's n on the degree of vegetation cover and -type as well as an influence of consecutive rainfall events. This finally leads to a more robust parameterization of near surface roughness for hydrodynamic modelling, which is particularly important for the simulation of heavy rainfall events.

1. Introduction

Flash floods resulting from torrential rainfall events can cause great damage and loss of human lives, as numerous events in Central Europe in recent years have demonstrated (Kaiser et al., 2020). While climate change is potentially increasing the intensity and frequency of such events, maps depicting the expected flooding risk caused by heavy rainfall are becoming increasingly important for communities (Sañudo et al., 2020; Bulti and Abebe, 2020). The use of detailed two-dimensional (2D) hydraulic models is the most common and accurate method for risk mapping (Rai et al., 2010).

The original purpose of hydraulic 2D-models is to simulate fluvial flood events, where the river overflows its bank. Meanwhile, the direct generation of surface runoff within a hydraulic model, considering hydrological processes like infiltration excess, has become also a standard use case (Zhang and Cundy, 1989; Fernández-Pato et al., 2016; Savant et al., 2019; David and Schmalz, 2020).

Using hydraulic 2D-models for heavy rainfall simulations, the precipitation is distributed over the model domain. This means that an individual amount of rain is added to each mesh-node or cell depending on the infiltration approach. Subsequently, the discharge concentration in flow paths caused by the surface topology is determined by solving the shallow water equations. This enables the creation of accurate flood maps showing endangered critical infrastructure or buildings. In contrast to fluvial flood simulations, these simulations can show hazards far away from water bodies caused by short and intense rainfall events.

Beside the hydrologic parameters, the flow resistance expressed by the surface roughness is the key parameter for 2D hydraulic surface runoff simulations (Rai et al., 2010; Barros and Colello, 2001). The

* Corresponding author at: Karlsruhe Institute of Technology, Campus Alpin, Kreuzeckbahnstraße 19, Garmisch-Partenkirchen, 82467, Germany.
E-mail address: patrick.laux@kit.edu (P. Laux).

https://doi.org/10.1016/j.jhydrol.2022.128786
Received 25 May 2022; Received in revised form 1 November 2022; Accepted 4 November 2022
Available online 1 December 2022

definition of the term roughness varies depending on the discipline and question. It can represent surface or flow properties, or simply serve as a model parameter. The lack of a uniform parameterization and scale dependency complicates the subject. Since no single surface property can be defined as "the roughness", roughness primarily reflects the accuracy of the measurement technique and the motivation for parameterization (Smith, 2014). The obstructive effects of roughness determine the velocity of the runoff on the surface and therefore the formation speed of a flood wave. In general, a smooth surface leads to a more rapidly rising flood wave, while peak discharge can be significantly lower on rough surfaces (Sanz-Ramos et al., 2021).

Vegetation coverage has the most significant effect on near surface runoff processes and surface resistance. Studies differentiate by vegetation type, flexibility, degree of submergence (Cantisani et al., 2014) or vegetation stem diameter (Zhang et al., 2021). A distinction is also often made between submerged and partially submerged vegetation (Kim et al., 2012; Wu et al., 1999).

Roughness implies the effects on flow by crop ridges, rocks, tillage, and the frictional drag over the surface (Engman, 1986). Romkens and Wang (1986) distinguish surface roughness into four categories: The first category includes microrelief variations in the range of 1–2 mm as the friction drag of the surface. The second type results from non-directional clumping of the soil as it arises, for example, from tillage in the range of 100 to 200 mm. The third class represents systematic or directional differences, such as plough tracks. The fourth type contains non-directional variations of the terrain with elevation differences. The increasing availability of high resolution terrain data, often with a horizontal resolution of less than 1 m and a vertical accuracy of a few centimetres, allows to depict most of the topographic complexity directly from the terrain model. The roughness parameterization has to represent all processes which lie beyond the terrain resolution as different flow processes occur at different topographic scales. So roughness parameterization has a scale dependency and parameters have to be chosen in dependency of the computational mesh resolution (Lane, 2005; Horritt et al., 2006).

The roughness of arable land is particularly difficult to standardize (Huang and Bradford, 1992; Sepaskhah and Bondar, 2002). Huang and Bradford (1992) demonstrated this with laboratory tests experimenting with different rain intensities and successive rain events. After an initial rainfall event of 63 mm, soil was crusted and roughness reduced. After a simulated rain event of 92 mm thereafter, microrills developed and the visible roughness of the surface increased due to its stronger structuring, whereby the roughness relevant to the runoff had decreased due to a channelling of the runoff.

The most common representation of roughness is done by the use of the Manning parameter (n) (Manning, 1891) as a value between 1 and 0. There are widely accepted and generally valid roughness coefficients for larger flow depths, such as those that occur during fluvial floods (Chow, 1959). Apart from this the roughness at shallow water depths is subject to greater uncertainties. Especially surface runoff simulations require a reliable choice of roughness parameters due to the high sensitivity of the results (Gaur and Mathur, 2003; Sauer and Ortlepp, 2021) and thus, possibly to errors in risk assessment of flash floods.

Many studies tried to find a relation with dimensionless parameters between Reynolds number or Froude number and vegetation or slope (Chow, 1959; Emmett, 1970; Wu et al., 1999; Díaz, 2005). Meanwhile, the use of water depth-dependent roughness relations rather than a single value representing the range of possible roughness effects for the simulation of surface runoff has become a standard in engineering (Gaur and Mathur, 2003; Rai et al., 2010; Mügler et al., 2011; Fraga et al., 2013). In practice, the application of roughness coefficients is a definition of a water depth-dependent relationship, as it is, for example, the case for the 2D-model HYDRO_AS-2D (Hydrotec, 2022). These models originally developed for river hydraulics make use of the Manning formula which is also the most common and widely used approach to quantify flow velocity (Díaz, 2005). Díaz (2005) divides the research concerning the Manning formula in two fields: the first type tries to develop new or extend existing formulas for the calculation of flow resistance as the formulation of the Manning formula is based only on empirical assumptions (Jarrett, 1990). The second type tries to determine better or more exact coefficients valid for specific use cases and conditions (Wu et al., 1999; Lawrence, 2000; Wilson and Horritt, 2002; Ding et al., 2004).

In this study, we contribute to the second type of research studies. Based on existing artificial rainfall experiments (Ries et al., 2020), we derive empirical parameters describing depth-dependent roughness relations valid for the micro topography and different land-use types. We use four different formulations describing roughness in order to compare their suitability for the proposed task. Combined with further data from literature, this leads to a better, more universal representation of overland flow in 2D-hydraulic models. Finally, this allows a more accurate assessment of flash flood risks and therefore, a better planning of counter measures.

To achieve this goal, an idealized hydraulic 2D-model is applied representing the test sites of the artificial rainfall experiments. By examining all possible parameter combinations to maximize the Nash Sutcliffe Efficiency (NSE) between observed and simulated discharge and a comparison with results from other experiments, a range of valid values is determined. In addition, the framework offers a way to determine roughness coefficients knowing only discharge, rainfall rate and slope of the test sites, thus avoiding complex measurements of water level or velocity.

2. Materials and methods

2.1. Artificial rainfall experiments

Artificial rainfall experiments are one option to examine roughness coefficients on real surfaces outside a laboratory. Ries et al. (2019) and Seibert et al. (2011), for example, provide collections of these experiments. In most cases, sprinkling experiments use a constant rain intensity (e.g., 70 mm/h), which corresponds to a statistical return interval for a local heavy rainfall event (e.g., a 100-year event). The water is sprayed via a sprinkling system over a defined period of time (e.g., 1 h) onto the test field. Simultaneously, the outflow is measured at the lower boundary of the test field as the volume of water running downstream as surface runoff in a high temporal resolution. The data set provided by Ries et al. (2019), for instance, includes the entire hydrograph with ascending and descending parts, whereas the collection of Seibert et al. (2011) does not include the descent of the hydrograph.

Sprinkling experiments with tracers (Tatard et al., 2008; Mügler et al., 2011) try to circumvent the problem of lacking flow velocity data by measuring the propagation rate of a tracer substance. A similar approach with a sprinkling setup to simulate rainfall has been conducted by Katz et al. (1995) using fluorescent dye and a slow motion camera system in an artificial channel to estimate flow velocities. However, these approaches focused mainly on one test site and did not cover a greater variety of surface properties. This lack of a sufficient quantity of data does not allow a comparison of multiple land cover types and therefore, artificial rainfall experiments with flow velocity measurements are not considered in this study.

One of the most comprehensive data sets available for Germany is provided by Ries et al. (2019). The artificial rainfall experiments took place at 23 locations in Baden-Wuerttemberg (Germany) with different vegetation and soil conditions on a defined field of 10 m length. Six experiments were conducted on each field, each with different rainfall duration, intensity and initial soil moisture. The following information was logged in a one minute time interval, which is relevant for our study:

- discharge at the lower end of the test field

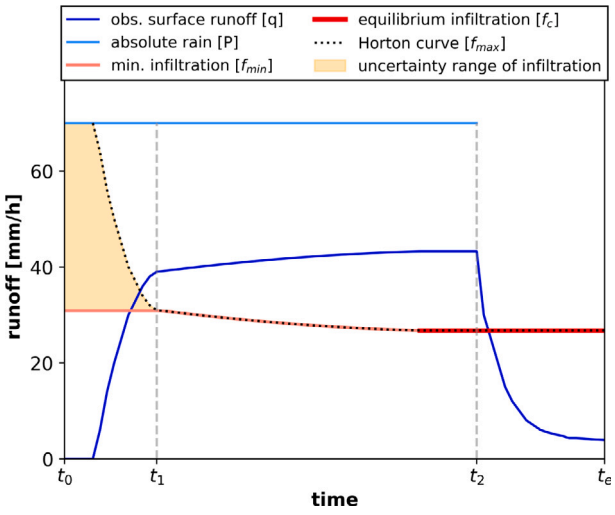

Fig. 1. Water fluxes in a schematic sprinkling experiment.

- rain intensity on the test field
- soil moisture at three different depths in the test field

Vegetation density [%] (0–100%), -height [m] (0–0.3 m), land-use (pasture, arable land), and slope [%] (9–32%) of each site have been documented. A detailed description of the experimental setup can be found in Ries et al. (2020).

2.2. The partitioning of roughness and infiltration

The basic idea is to use the shape of the hydrograph to infer the roughness of the surface. The shape of the hydrograph is generally dependent on precipitation rate, infiltration rate and roughness. As precipitation rate P [mm/h] is constant, the partitioning of runoff q [mm/h], infiltration f [mm/h] and roughness is the key for determining Manning's n [$sm^{-\frac{1}{3}}$]. The relevant fluxes can be seen in the schematic drawing of a fictive sprinkling experiment in Fig. 1.

The partitioning of runoff and infiltration changes during the rainfall experiment. This behaviour is not only caused by changes in soil moisture but also from rainfall induced surface sealing (Assouline, 2004). The impact of raindrops causes surface sealing by the destruction of soil aggregates, which reduces the soil porosity by siltation (McIntyre, 1958; Farres, 1978). Also chemical dispersion depending on the chemistry of the soil affects sealing (Agassi et al., 1996). Soil sealing is a crucial process for surfaces with low vegetation cover, as the soil becomes less and less permeable caused by rapidly transforming soil surface features with persistent or consecutive rain events (Bresson and Boiffin, 1990; Ribolzi et al., 2011). In addition, Ribolzi et al. (2011) stated that high intensity rain on surfaces with a slope gradient less than 30% (which is the case for the data) leads to less permeable erosion crusts, while higher slopes cause more permeable structures.

Consequently the change of infiltration rate over time is a non-linear curve and must be considered for each rainfall experiment individually. Most equations describing the infiltration process are monotonically decreasing functions based on power laws or exponential decays (Assouline, 2013). To describe the infiltration process of the artificial rainfall experiments, a Hortonian depletion curve (Horton, 1933; Beven, 2004) is used to calculate the maximum possible infiltration rate f_{max} of the rainfall experiment by fitting the equation to the difference of rainfall and observed discharge. The minimum possible infiltration rate f_{min} can be estimated, when the hydrograph is nearly constant. The actual infiltration rate f lies between the maximum and minimum infiltration rate, which implies that f can only be determined when $f_{max} = f_{min}$. The empirical Horton equation decreases f_{max} exponentially from its initial value f_0 to its final one f_c, using the decay coefficient α (Eq. (1)).

$$f(t) = f_c + (f_0 - f_c)e^{-\alpha t} \tag{1}$$

The variables of the Horton function are calculated with the non-linear least square method as proposed by Esen (1987) to fit the function (Eq. (1)) to the observed data. The applied method using the Levenberg–Marquardt algorithm is implemented in the MINPACK-1 package (Moré et al., 1980). A Horton curve is displayed exemplarily in Fig. 1 as maximum possible infiltration rate f_{max}.

The schematic artificial rainfall experiment can be separated in three time segments: Ascent of the hydrograph, nearly constant discharge and descent of the hydrograph. During the ascent of the hydrograph, the infiltration cannot be determined unambiguously (orange area in Fig. 1), as the physical process of soil saturation is not represented by the empirical Horton approach. Consequently the impact of Manning's n on the shape of the hydrograph cannot be separated from infiltration, since q is a function of f, Manning's n and precipitation P (Eq. (2)).

$$dq/dt > 0 \quad and \quad q_{t_0 \le t \le t_1} = F(f, n, P) \tag{2}$$

A constant wetting rate leads to a gradually increasing q and converges in many observed cases to a steady rate. The observed soil moisture data (not shown) shows also a plateau leading to the conclusion, that the maximum saturation has been reached, the depression storage is filled and infiltration into the soil is constant. Infiltration before the termination of artificial rainfall f_{min} is in many cases equivalent to the equilibrium infiltration rate f_c resulting in a constant surface runoff. So infiltration is clearly predictable for these cases as a difference between precipitation P and discharge q. But no inference on n can be made in this time segment, as roughness has no visible effect on the hydrograph, because runoff is nearly constant (Eq. (3)).

$$dq/dt \cong 0 \quad and \quad q_{t_1 \le t \le t_2} = F(f_c, P) \tag{3}$$

Finally, the third time segment begins with the cessation of rainfall resulting in the descent of the hydrograph. The decreasing q is a function of f and n (Eq. (4)).

$$dq/dt < 0 \quad and \quad q_{t_2 \le t \le t_e} = F(f, n) \tag{4}$$

A nearly constant infiltration rate can be extrapolated by using the fitted Horton function for the falling limb segment of the hydrograph. Consequently the impact of n on the shape of this segment of the hydrograph can finally be separated from infiltration, allowing a clear determination of roughness.

In addition, high roughness coefficients cause a slower ascending hydrograph. This effect can be used to verify the estimated n, excluding roughness coefficients leading to a simulated slower rise of the hydrograph simultaneously applying the minimum infiltration rate $f_{\min}$ in the model (Eq. (5)).

$$Qsim_{t_0 \le t \le t_1} \ge F(P, n, f_{\min}) \tag{5}$$

The collection of rainfall experiments provides a large variety of different hydrographs with maximum discharge ranging from 5 to 150 mm/h. No meaningful roughness can be derived from experiments with very low discharges. To recalculate the observed hydrograph, a comparatively much higher roughness would be needed, partly even with a Manning value greater than 1. This is presumably caused by continuous drainage of soil and vegetation, distorting the hydrograph. For this reason, experiments whose discharge does not exceed 15 mm/h are generally excluded and discharge values below 5 mm/h are not considered in the comparison of simulated and observed discharge.

2.3. Numerical hydraulic model

For one-dimensional and stationary conditions, discharge q [$\frac{m^3}{sm}$] can be calculated under consideration of roughness as followed according to the converted Manning equation (Eq. (6)) (Manning, 1891).

$$q = \frac{1}{n} \times h^{\frac{5}{3}} \times \sqrt{S_f} \tag{6}$$

During the artificial rainfall experiments only q has been measured as integral value and the energy slope S_f is known as a property of the respective site. So Manning's equation does not allow an unambiguous calculation of q, as it can be determined with different roughness coefficients n and their respective flow depth h. In addition, the instationary distribution of flow depth (Fig. 2) cannot be represented by the Manning equation, as well as the ascent and descent of the hydrograph, due to water accumulation to the end of the experimental site. So the flow processes must be calculated by a two-dimensional approach.

Calculation of instationary flow on a surface is based on the two-dimensional depth-averaged flow equations (shallow water equations). They integrate the three-dimensional continuity equation and the Reynolds-averaged-Navier–Stokes equations for incompressible fluids over the water depth by assuming hydrostatic pressure distribution (Pironneau, 1988). The shallow water equations in compact vector format are defined as followed:

$$\frac{\delta \boldsymbol{w}}{\delta t} + \frac{\delta \boldsymbol{f}}{\delta x} + \frac{\delta \boldsymbol{g}}{\delta y} + \boldsymbol{s} = 0 \tag{7}$$

with:

$$\boldsymbol{w} = \begin{bmatrix} H \\ uh \\ vh \end{bmatrix} \tag{8}$$

$$\boldsymbol{f} = \begin{bmatrix} uh \\ u^2h + 0.5gh^2 - vh\frac{\delta u}{\delta x} \\ uvh - vh\frac{\delta v}{\delta x} \end{bmatrix} \tag{9}$$

$$\boldsymbol{s} = \begin{bmatrix} 0 \\ gh(S_{fx} - S_{bx}) \\ gh(S_{fy} - S_{by}) \end{bmatrix} \tag{10}$$

$$\boldsymbol{g} = \begin{bmatrix} vh \\ uvh - vh\frac{\delta u}{\delta y} \\ v^2h + 0.5h^2 - vh\frac{\delta v}{\delta y} \end{bmatrix} \tag{11}$$

$H = h+z$ which represents the water level as the sum of water depth (h) and elevation of the surface (z). u and v are the velocity components in x- and y-direction. The source term s involves the friction slope $\boldsymbol{S}_f$ (with the components S_{fx} and S_{fy}) and the bed slope (S_{bx}, S_{by}). The slope of the surface (bed slope) is defined by the gradient of bed level z in x and y direction:

$$S_{bx} = \frac{-\delta z}{\delta x}, S_{by} = \frac{-\delta z}{\delta y} \tag{12}$$

The friction slope S_f is calculated with the Darcy-Weisbach equation:

$$S_f = \frac{\lambda \boldsymbol{v}\,|\boldsymbol{v}|}{2gD} \tag{13}$$

With the Manning equation the friction factor λ is determined:

$$\lambda = 6.34\frac{2gn^2}{D^{1/3}} \tag{14}$$

g is defined as earth gravity and $D = 4r_{hy}$ is representing the hydraulic diameter. Applying the 2D shallow water equations the hydraulic radius r_{hy} is equivalent to the water depth h. Using the finite volume method the shown equations provide depth and flow velocity at each node of the computational mesh in a temporal resolution. For our study, we used the hydrodynamic model HYDRO_AS-2D (Hydrotec, 2022). The model HYDRO_AS-2D is widely used in Germany and is applied both for the simulation of fluvial flood events and for surface runoff caused by heavy rainfall. The discharge calculation is carried out via the finite volume method, based on a mesh consisting of triangles and quadrilaterals. The use of a combined mesh of triangles and quadrilaterals allows an easier adaptation to the topographical and hydrodynamic conditions of the respective task. In a standard use case, the structure of the hydraulic model is based on laserscan data. The model representing the test sites consists of an inclined plane, whose slope is specified in the database (Fig. 2).

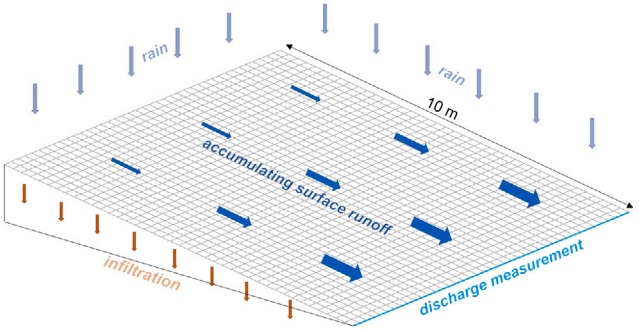

Fig. 2. Illustration of the model domain displayed as rectangular cells in combination with the simulated water fluxes.

As the test sites are homogeneous areas, microtopography is not considered as height variation in the computational mesh. The surface roughness is modelled with water depth-dependent or constant Manning coefficients on each node. So all flow affecting parameters like microtopography, vegetation resistance, splash effects of raindrops or rill formation due to erosion must be represented by the roughness coefficient.

Corresponding to the real experiments, the surface of the model has a length of 10 m. The width of the site is not relevant, because flow is measured in discharge per metre. The selection of a sufficient number of nodes has been done by a sensitivity analysis leading to an optimal node spacing of 25 cm. This is the key to exclude an influence of model discretization on the results. The rain is modelled via so-called source-nodes as a spatial homogeneous addition of water. The infiltration is modelled similarly to the rain as negative source-nodes, if necessary, in a time dependent manner. The advantage of this procedure in comparison to a simple reduction of the amount of rainfall is that the infiltration can be active while or after the rainfall. At the lower end of the surface, the discharge and the water level is logged for further analysis.

2.4. Reducing the solution space

Each experiment leads to a solution space representing several acceptable roughness functions with minimal difference in quality of the results. Comparing the solution spaces of experiments with similar properties, overlapping areas can be obtained leading to the assumption, that there must be a smaller general valid solution space.

Three steps are now taken to reduce the solution space. The first step is to exclude smooth (low n) roughness relations based on the ascending hydrograph as described in Section 2.2. In the second step, the individual experiments of one site are compared with each other to find similarities, that are valid for all. Finally, the remaining solution space can be compared to sites with similar properties to further reduce or verify the results. Fig. 3 shows the described process schematically.

The method followed in this study for determining the roughness coefficient is the iterative testing of different roughness values and the subsequent comparison of the hydrographs using a statistical performance measure like the Nash Sutcliffe Efficiency (NSE). The identified roughness coefficients with a high NSE score can be compared to the

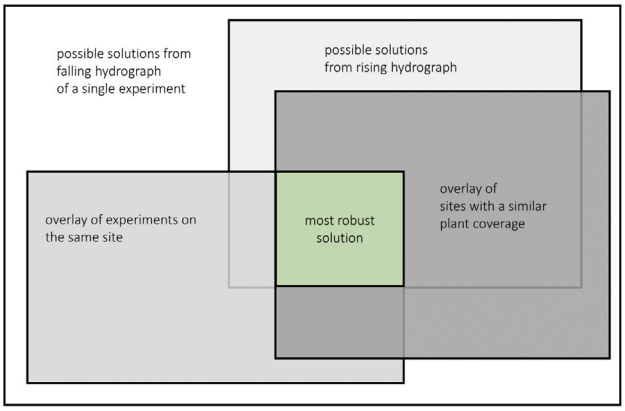

Fig. 3. Framework for reducing the solution space.

other experiments with different rain and infiltration rates of the same test site. If all experiments lead to a similar roughness value, the result can be considered as robust solution.

2.5. Roughness functions

Three depth dependent formulations of near surface roughness and one depth independent approach with different advantages are used to parameterize the roughness function to prove the robustness of the presented framework.

2.5.1. Constant roughness coefficients

The use of constant (depth independent) roughness coefficients is the most straightforward method. For this use case, no parameterization is needed, but the Manning values can be iterated directly within the framework.

2.5.2. Exponential function

Thus, better fitting shapes of the hydrographs and a universally valid roughness can only be modelled with depth-dependent roughness relationships. This assumption is confirmed by many authors (Wu, 2008; Fraga et al., 2013; Rai et al., 2010; Mügler et al., 2011; Fu et al., 2019). To describe depth-dependent roughness we parameterize n as a reciprocal *exponential function* of h defined by the variables c and d (Eq. (15)).

$$n = \frac{1}{c + e^{dh}} \tag{15}$$

The possible representation of either a constant roughness ($d = 0$) or a depth-dependent ($d > 0$) decreasing roughness with increasing water depth is the advantage of this function. This allows to test all possible combinations of the variables c and d in a reasonable range of values and to compare the observed with the simulated falling limb of the hydrograph. The reciprocal is used to achieve a better distribution of roughness functions, as functions with a low n would otherwise be underrepresented, if c and d are iterated linearly. Preliminary test simulation showed that the differences in the simulated hydrograph of a linear varied n with high roughness values (0.6 to 1.0) are less pronounced than with a smaller n (0.2 to 0.4). The *exponential function* has no direct link to Manning's equation, but covers all possible variations of decreasing roughness with increasing water depth.

2.5.3. Kadlec's Power Law

Experimental investigations studying the shallow overland flow found a relationship between vegetative drag and roughness coefficient (Kadlec, 1990; Wu et al., 1999; Tsihrintzis et al., 2001; Gaur and Mathur, 2003). On the basis of these findings Jain et al. (2004) simplified *Kadlec's Power Law* for the application in a distributed rainfall model (Eq. (16)).

$$n = n_0 \left(\frac{h}{h_0}\right)^{-\epsilon} \tag{16}$$

with the limits: $h < h_0$ and $n = n_0$ for $h \geq h_0$ h_0 defines minimum flow depth, beyond which the roughness coefficient n_0 is assumed constant. The exponent ϵ represents the influence of vegetation drag. This formulation of a depth-dependent roughness function is well established and has been used in several studies (Mügler et al., 2011; Simons et al., 2014; Özgen et al., 2015). The formulation is opposite to the exponential function, since it emphasizes low roughness more strongly for a linear iteration of n_0. The simplified Power Law can result in a decreasing or increasing function and has therefore, a wider range of possible solutions.

2.5.4. Fu's equation

A newer formulation describing depth-dependent roughness based on the Manning equation has been provided by Fu et al. (2019). Later the equation has been adapted to be valid for litter cover (Ding et al., 2021). Fu conducted several laboratory experiments for a vegetation cover from 0 to 30% with artificial plants with a height of 12 cm. *Fu's equation* leads to a nearly constant roughness for low vegetation cover and an increasing roughness with higher water depths for a higher vegetation cover. The equation calculates Manning's roughness on stem covered slopes and shows that the influence of plant stem resistance, flow resistance from vegetation and boundary resistance depends on water depth and plant basal cover (C_v). C_v is defined as the ratio between the area covered by stems (A_s) and flume bed (A_f) (Eq. (17)).

$$C_v = 100 A_s / A_f \tag{17}$$

C_v is regarded as equivalent to the plant coverage documented by Ries et al. (2020) as no further information about the methodology is provided. The coefficients a and b vary with vegetation type (Eq. (18) as provided by Fu et al. (2019)).

$$n = (a + b(1 - e^{-0.061 C_v})^{1.668}) h^{0.604 - 0.710 e^{-0.219 Cv}} \tag{18}$$

The solution space of Fu's equation is limited, because the shape of the function is mainly defined by the vegetation coverage. The advantage is, that this reduces the necessary number of possible iterations to find a solution, but this could also result in a lack of accuracy. Fu's equation has been determined with relatively low stem covers (<30%) and flow depths larger than 0.5 cm. So the validity for higher vegetation covers, the transferability of Fu's stem cover to vegetation cover, as used in the data of Ries et al. (2019), and lower flow depth needs to be verified.

3. Results

The calibration of the three equations leads to multiple water depth-dependent roughness functions and therefore to differing hydrographs. Similarity of the resulting falling limb of the simulated hydrograph with the measured one is represented by the NSE as a value between 0 and 1.

3.1. The most robust result

The result is a heat map where each raster cell stands for one depth-dependent roughness relation and the quality of its comparison to the descending part of the hydrograph. 22 sites out of 23 are useable for simulation (Table 1), since no runoff could be generated at site 10 with any artificial rainfall experiment due to high soil porosity. For each site, up to six matrices, depending on the number of useable

Table 1
Overview of the most robust parameter combinations together with the relevant properties of their respective experimental sites.

Site	Cv[a]	S[a]	Veg. type[a]	const. n	exp. function				Kadlec's Power Law				Fu's equation			
	[%]	[%]		n	c	d	n^b	h^c [mm]	n_0	ϵ	n^b	h^c [mm]	a	b	n^b	h^c [mm]
1	100	12	Pasture	0.58	0.70	0.59	0.59	5	0.250	0.45	0.47	5	0.3	0.50	0.57	5
2	100	18	Pasture	0.60	0.50	0.63	0.63	5	0.825	0.05	0.88	7	0.8	0.00	0.57	5
3	90	16	Pasture	0.70	0.40	0.69	0.69	6	0.575	0.10	0.66	6	0.7	0.25	0.68	6
4	40	16	Mustard	0.45	0.40	0.53	0.53	5	0.600	−0.15	0.49	5	0.6	0.00	0.43	4
5	0	14	Triticale (seeded)	0.18	3.90	0.20	0.20	4	0.100	0.40	0.17	3	0.0	0.75	0.11	3
6	100	21	Pasture	0.65	0.40	0.67	0.67	5	0.975	0.00	0.97	6	0.6	0.25	0.61	4
7	80	14	Winter barley	0.38	0.20	0.44	0.44	3	0.550	−0.20	0.42	3	0.5	0.00	0.36	3
8	15	16	Corn (seeded)	0.13	7.00	0.12	0.12	3	0.125	−0.20	0.09	2	0.0	0.25	0.09	2
9	100	21	Pasture	0.58	0.40	0.64	0.64	5	0.650	−0.05	0.61	5	0.8	0.00	0.57	5
10	100	32	Pasture	–	–	–	–	–	–	–	–	–	–	–	–	–
11	80	18	Pasture	0.68	0.00	0.82	0.82	5	0.750	−0.05	0.70	4	0.4	0.50	0.64	4
12	100	19	Pasture	0.65	0.40	0.67	0.67	4	0.500	0.15	0.62	4	0.6	0.25	0.61	4
13	40	11	Alfalfa	0.28	1.40	0.28	0.28	2	0.475	−0.30	0.31	2	0.4	0.00	0.29	2
14	100	27	Pasture	0.70	0.00	0.82	0.82	5	0.800	−0.05	0.75	5	–	–	–	–
15	0	14	Winter barley	0.50	0.00	0.62	0.62	3	0.225	0.40	0.39	3	0.0	0.75	0.11	2
16	100	12	Pasture	0.40	1.60	0.38	0.38	4	0.550	−0.25	0.39	4	0.5	0.00	0.36	3
17	100	14	Pasture	0.48	0.50	0.53	0.53	5	0.575	−0.10	0.50	5	0.4	0.25	0.46	5
18	60	12	Alfalfa and clover	0.38	1.50	0.39	0.39	4	0.250	0.20	0.33	4	0.5	0.00	0.36	4
19	100	21	Pasture	0.98	0.00	1.00	1.00	6	0.975	0.00	0.97	6	1.0	0.25	0.89	6
20	0	9	Corn (harvested)	0.05	19.50	0.01	0.01	1	0.050	0.00	0.05	2	0.0	0.25	0.04	2
21	50	14	Green manure	0.35	1.30	0.37	0.37	3	0.525	−0.20	0.40	3	0.0	0.50	0.33	3
22	100	12	Pasture	0.38	1.60	0.38	0.38	4	0.175	0.50	0.35	3	0.3	0.25	0.39	4
23	0	14	Corn (harvested)	0.08	7.00	0.10	0.10	2	0.125	−0.10	0.11	2	0.0	0.50	0.07	2

[a]Data taken from Ries et al. (2019).
[b]Manning's n [$sm^{-\frac{1}{3}}$] at a water depth of 4 mm.
[c]Maximum water depth during simulation.

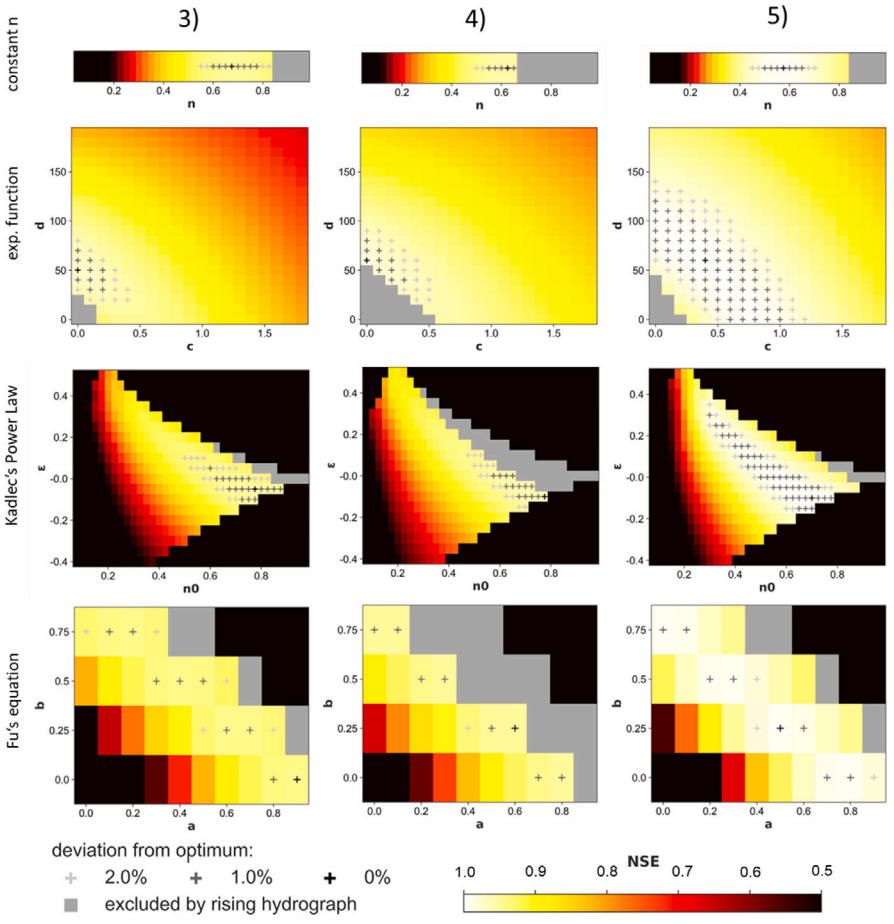

Fig. 4. Matrices of NSE values of the experiments 3, 4 and 5 on site 9 conducted with a constant n, the exponential function, Kadlec's Power Law and Fu's equation. The crosses highlight the roughness relations with the smallest deviation from the optimum. The grey marked cells can be excluded as simulated q is smaller than the rising hydrograph due to too high roughness as described in Section 2.2.

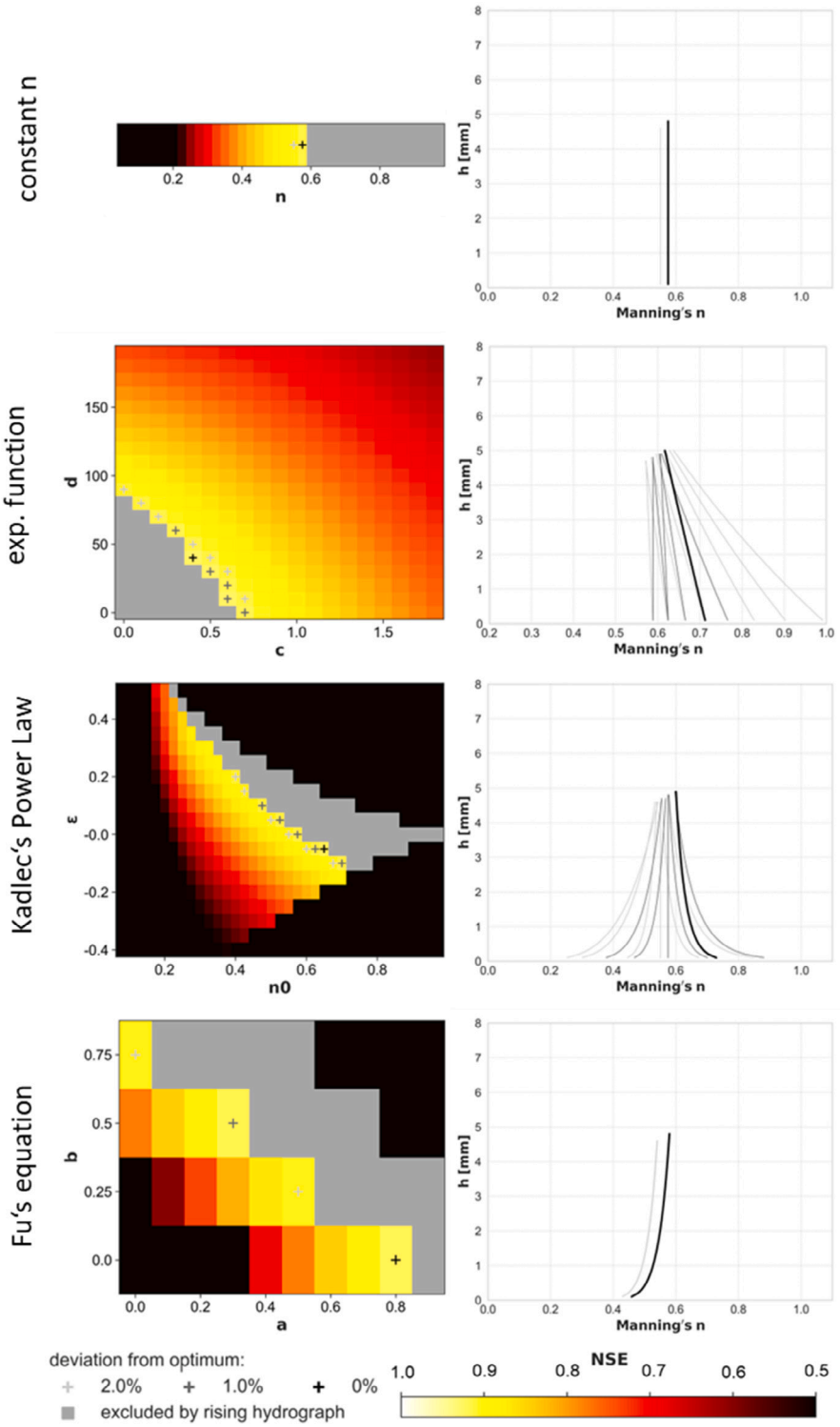

Fig. 5. left: Minimum NSE of all six simulatable experiments of site 9. **right:** Resulting depth dependent roughness functions as indicated by the crosses.

experiments, are generated. The number of useable experiments depends on the successful generation of surface runoff. In many cases, the first experiment or experiments with a short rainfall duration did not produce any runoff, because soil moisture could not sufficiently build up. Fig. 4 exemplarily shows the matrices of three out of six experiments simulated for site 9 (100% veg. cover).

The crosses in the heat maps demonstrate the deviation from the highest NSE value and are an indicator for the ambiguousness of the results of one experiment. Thus, coherent and similar areas with crosses indicate robust solution spaces. The more crosses appear, the more possible parameter combinations lead to a good result. To reduce the number of solutions, an overlay of the results of all experiments of one site is performed. By calculating the minimum NSE values of each parameter combination (Fig. 5), the lowest common denominator representing a solution, which is most acceptable for all experiments, can be found. In order to verify the selection of the minimum as best possible solution, the optimum solution space is compared with the optimum of other statistical moments, such as mean, median, standard

deviation, or coefficient of variation (not shown). All the statistical moments of NSE lead to similar results, as well as the simulated hydrographs resemble to the observed ones. But the minimum is considered as the most robust solution between the different experiments. Taking the mean values, for instance, would not assure that all the experiments are contained in the optimum solution space.

On site 9 basically all four approaches lead to a range of n values between 0.5 and 0.7 (Fig. 5). The exponential function and Kadlec's Power Law result in similar optimum roughness functions (black lines) with n-values decreasing with h. But the solution space (grey functions) of Kadlec's Power Law covers also the optimum solution derived with Fu's equation. The formulation of Fu's equation determines an increasing n with flow depth for higher vegetation coverage due to its predefined properties and does not allow much variation for full vegetation coverage. Accordingly all $a-b$ combinations generate similar results, as the functions in Fig. 5 overlap each other. The optimum depth dependent functions differ to a minor degree from the constant roughness as the flow process takes in this case completely place in partially submerged vegetation. Therefore also the constant approach results in a high NSE value, while the overall best fitting function leads to a slightly decreasing n with h.

The resulting parameters together with the most important properties of their sites are listed in Table 1.

To enable a straightforward comparison of the results, the n-value of each function at a depth of 4 mm is listed. To indicate the limitation of the respective function, the highest flow depth (h) achieved during the numeric simulation is also presented. Since the maximum flow depth of some functions (e.g. sites 13, 20 and 23) lies significantly below 4 mm, they can nonetheless be seen as valid, as they show a nearly constant n, which can be extrapolated to 4 mm.

3.2. Numerical and experimental hydrographs

The comparison between the observed and the simulated falling limb of the hydrographs, obtained from applying the four roughness approaches in the hydraulic model in Fig. 6, lead to nearly identical results (NSE values from 0.94 to 0.99). The respective minimum NSE is equivalent to the optimum value derived from the overlay in Fig. 5. The NSE values of the single experiments correspond to the values presented in Fig. 4 and the position determined by the optimum value. The simulation has been conducted with the in Section 2.2 described minimum infiltration rate f_{min}.

The criteria for an acceptable shape of a simulated hydrograph is defined as followed: First, the rise of the simulated hydrograph must be higher or equal to the observed q, since infiltration is modelled as the minimum obtained from fitting the difference of precipitation and discharge to the Horton function. Second, the simulated descent of the hydrograph must fit to the observed data. Some deviation at the lower end is tolerable, as this is assumed to be caused by soil or vegetation draining effects, which cannot be mapped by the roughness formulation. The example of site 9 shows, that these criteria can be met, as well as high NSE coefficients can be achieved independently of the applied roughness formulation.

3.3. Quality and variability of the results

The quality of the results is shown in Fig. 7 comparing the achieved NSE values of the four approaches. High NSE values are achieved if the conducted rainfall experiments resulted in similar hydrographs, while low NSE values are caused by diverging discharge measurements. Site 19 is a negative exception because of extremely dense vegetation, so that even with a Manning value of 1, the hydrograph cannot be modelled correctly.

Considering all sites, it can be stated that Kadlec's Power Law gives the best results on average, since this formula reflects best the variability of the vegetation with increasing or decreasing roughness.

Table 2
Clusters obtained from the parameters calculated with Kadlec's Power Law.

Nr	Cluster (sites)	Common characteristics	NSE	n_0	ϵ
1	8, 20, 23	Low veg. cov., corn	0.87	0.075	−0.30
2	5, 15	Low veg. cov., grain	0.83	0.100	0.50
3	1, 22	Longer grass	0.89	0.200	0.45
4	3, 9, 12, 17	Shorter grass	0.91	0.650	0.05
5	4, 7, 13, 16, 21	Medium density field crops	0.88	0.500	−0.25
6	2, 6, 11, 14, 19	High density pasture	0.74	0.975	0.00

The exponential function also achieves a high level of consistency, unless on sites where the roughness is strongly increasing with flow depth (e.g. site 8 and 16).

Fu's equation tends to result in lower NSE values, since the adaptability of the formula is limited. Significantly lower results compared to Kadlec's Power Law are achieved on sites where roughness clearly decreases with water depth (e.g. sites 22 and 23). At the same time, less iterations are necessary to obtain reasonable results, since vegetation coverage is directly considered in the formulation. Executing a higher number of iterations with a finer parameter sampling interval could not improve the results significantly.

The quality of the results of constant n varies strongly with the properties of the respective site. Sites with a dense vegetation tend to have a less pronounced depth dependent roughness and therefore a low difference to the other approaches is achieved (e.g. sites 12, 14 and 22). In contrast to sites with low or no vegetation cover, the NSE values achieved with the constant n decrease significantly compared to the depth dependent approaches (e.g. sites 5, 8 and 23).

The variation of roughness is shown in Fig. 8 by comparing roughness at a depth of 4 mm with the results derived with Kadlec's Power Law.

Larger deviations occur mainly at the upper end of the scale. In particular, the comparison with Fu's equation shows a larger variance due to the lower adaptability of the formula. The variation compared to the exponential function is lower as both approaches lead in many cases to similar solutions. It is noticeable that the constant roughness has the smallest deviations. This can be explained by the considered the water depth of 4 mm, since the depth independent approach tends to result in a mean roughness value.

3.4. Correlation of parameters and site characteristics

In comparison to the other approaches, the strongest correlation between the parameters and vegetation cover could be ascertained with Kadlec's Power Law. Fig. 9 shows the identified $n_0-\epsilon$ values calculated with Kadlec's Power Law with a maximum deviation of 1% of their optimum in dependency of the degree of vegetation coverage. Low vegetation cover corresponds clearly with a low n_0 and an ϵ-value approaching zero resulting in a nearly constant roughness function. A more differentiated result is obtained focusing on medium vegetation cover (30–60%). Overall, the roughness function tends to become smoother with increasing flow depth, corresponding to a negative ϵ. Exceptions can be caused by different plant types, such as at site 18 with alfalfa and clover. High vegetation cover (>60%) results in many cases in a high n_0. Lower n_0 values are associated with a significantly positive ϵ corresponding to a rapidly increasing roughness with flow depth.

Going further into detail, different clusters with common vegetation characteristics can be obtained from the data (Table 2). To verify the coincidence of the cluster, the minimum NSE coefficient of the sites is calculated to find the best possible concordance, that is acceptable for all sites. For all clusters, an adequate parameter combination can be obtained, as the NSE values indicate. The high variability (low NSE) in high density pasture (cluster 6) can be substantiated with larger deviations in vegetation texture, since there are still major differences, even if vegetation coverage is assumed to be 100%.

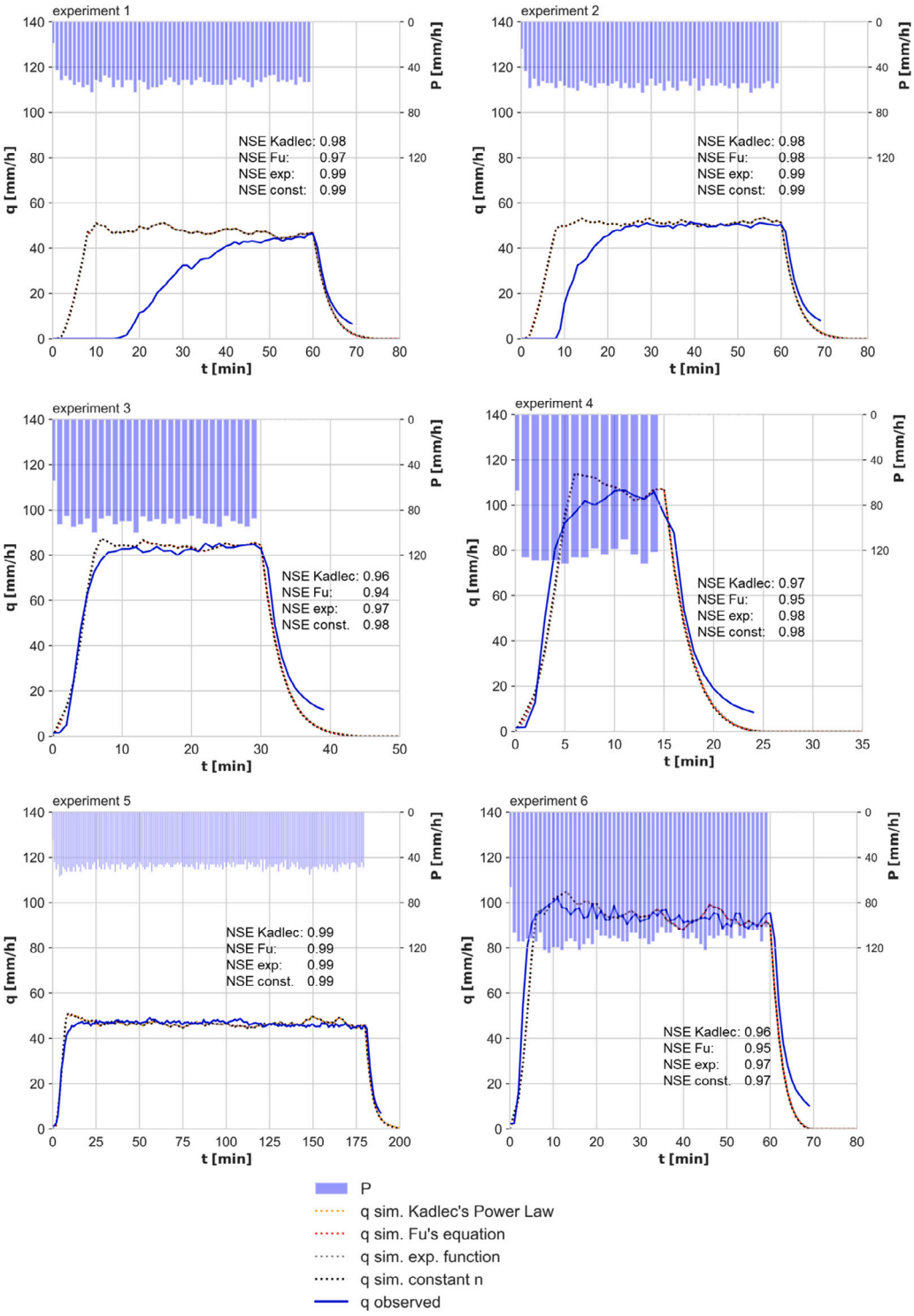

Fig. 6. Comparison of observed and simulated hydrographs of all six experiments of site 9. The NSE values assess only the falling limb of the hydrograph and discharge higher than 5 mm/h.

As Fu's equation implies vegetation cover directly, the parameters a and b should represent the plant type according to Fu et al. (2019). So an overlay summarizing plant types in order to calculate the minimum NSE value is conducted (Fig. 10). For the shown vegetation types, a best corresponding parameter combination could be determined. But it must be admitted that, for most of the plant types, experiments have been conducted only on one site. But as alfalfa, mustard and winter barley depict a cluster as well as the recently seeded or harvested types, the results can be seen as plausible. The most important information for hydraulic modelling is, that pasture, as a frequently applied land-use, can be classified by the use of the data of twelve sites resulting in a solution space around the indicated position of $a = 0.4$ and $b = 0.5$.

3.5. Roughness and consecutive rainfall events

Ribolzi et al. (2011) state, that consecutive rainfall may cause severe changes in the surface structure, especially for higher rain intensities on bare soil. This possibly affects the roughness coefficient. To visualize

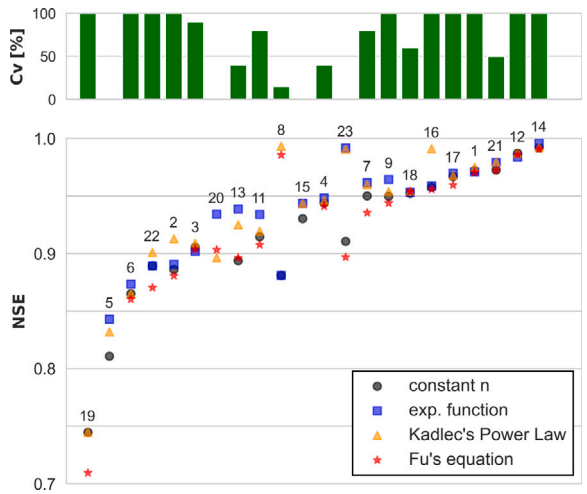

Fig. 7. Comparison of optimum NSE values, ordered by value and labelled with the respective site number. Green bars indicate the vegetation coverage [%] of the respective site.

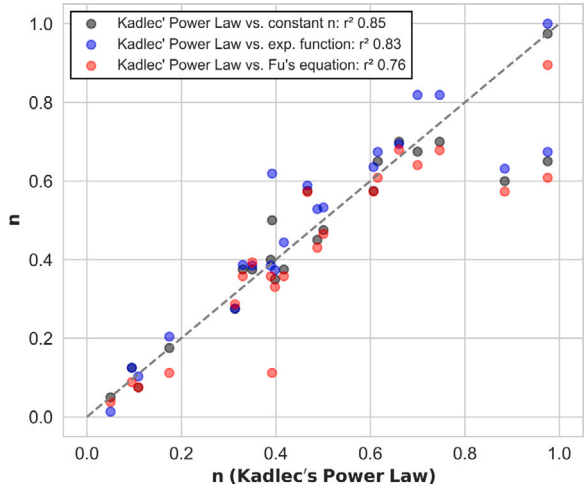

Fig. 8. Comparison of optimum n calculated with Kadlec's Power Law compared with the other three approaches at a flow depth of 4 mm.

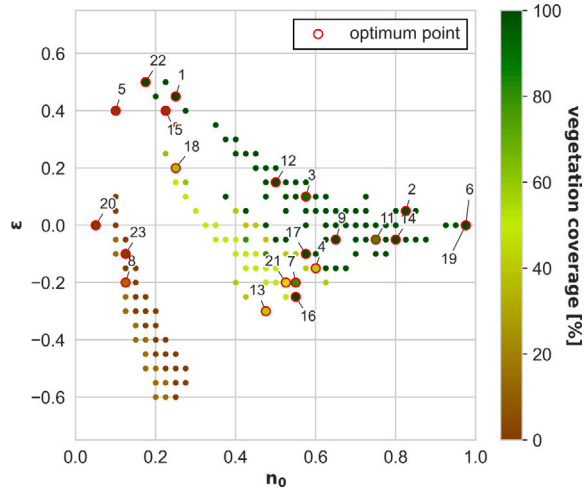

Fig. 9. $n_0 - \epsilon$ combinations calculated with Kadlec's Power Law with maximum 1% deviation from optimum point of the respective site.

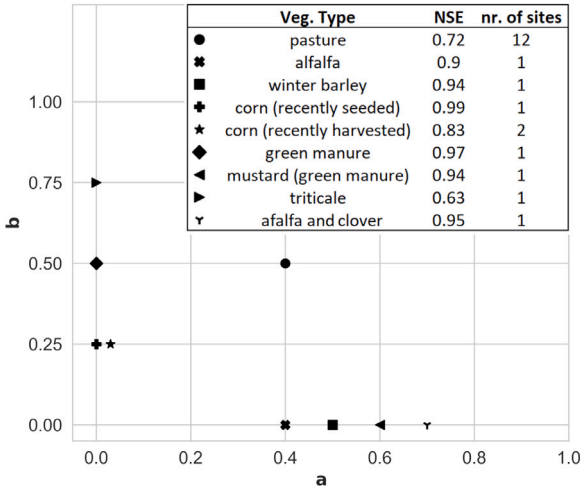

Fig. 10. Optimum $a - b$ combinations for Fu's equation classified according to vegetation type.

the effect of the consecutive rainfall experiments, the deviation from mean n of the experiments conducted at a site at a flow depth of 4 mm is calculated.

The consideration of a single site does not yet show a clear shift of roughness, but the comparison of all sites implies an influence of rain intensity and duration on roughness (Fig. 11).

The first and second experiment feature equal rainfall intensity and duration. The difference in the distribution of n is probably caused by the size of the sample. For the experiments 3 and especially 4, the rainfall duration was shorter while intensity has been increased. Here a shift towards a higher n can be recognized. In contrast to experiment 5 with a long duration and significant smaller rain intensity, the roughness decreases. The last experiment alters again towards a higher roughness. In conclusion, a general trend in shifting roughness towards one direction caused by consecutive rain experiments, as stated by Huang and Bradford (1992), cannot be recognized. Probably, the high variability in intensity and duration overlays this effect. But it can be concluded, that a high intensity and especially a short duration leads to significantly higher roughness values (exp. 4 and 6), while a long duration has the opposite effect (exp. 5). During longer rain events, more pronounced flow paths and grooves may develop, while the raindrop impact may increase roughness during shorter events (Fraga et al., 2013). The effect is slightly stronger on bare soil, but the sample size is not sufficient to make robust conclusions.

4. Discussion

Our study shows that the presented framework robustly determines roughness values from artificial rainfall experiments without data of flow velocity or water depth. Independently of the used method, all four applied approaches result in similar roughness functions, while they offer different advantages.

A constant roughness is the most straightforward formulation, but results only in valid values as long as the depth dependence is negligible, which is mainly the case for surface runoff in partially submerged vegetation.

The exponential function covers all possible decreasing or constant water depth functions and leads, in these cases, to accurate roughness relations. The disadvantage is, that there is no clear correlation between the calculated parameters and vegetation cover.

Kadlec's Power Law covers both, decreasing and increasing functions and therefore, delivers a wider range of functions. The results indicate, that increasing or decreasing functions are necessary to describe the near surface roughness as different vegetation types may

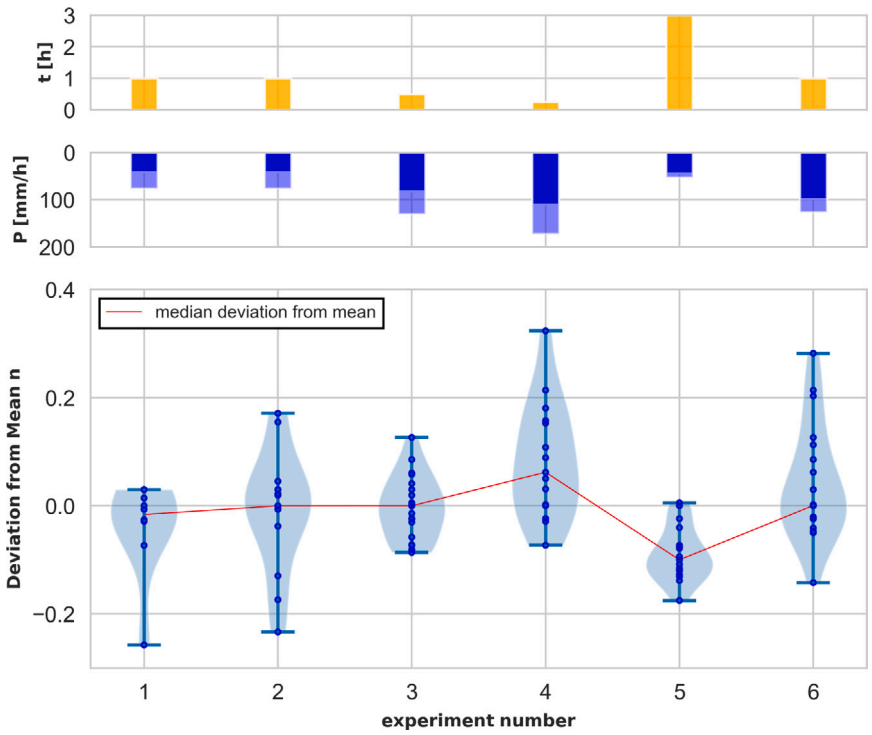

Fig. 11. Roughness variability caused by rainfall intensity and -duration. Top row: duration t of the rain experiments (orange bars). Middle row: precipitation intensity P (blue bars) combined with its variability (light blue bars). Bottom row: Deviation from mean n (at a flow depth of 4 mm) of the respective site. The distribution is shown by violin plots, while blue dots presents the number of samples. The red line shows the median of the distribution.

cause different shapes of the function. In addition a clear link between vegetation properties and the parameters could be recognized (Fig. 9 and Table 2)

Fu's equation, based on the Manning equation and empirical observations, needs much less iterations to find a suitable roughness function, as vegetation cover is directly implemented in the formulation. Fu et al. (2019) states that the parameters are dependent on plant type, which is confirmed by our results and valid parameters for the near surface can be provided (Fig. 10).

The result of the study are water depth-dependent or constant roughness relationships for water depths under 1 cm. Further research should generate higher water depths in field experiments, which can be achieved using longer test fields (in the range of 10 m or higher) or higher rain intensities. However, the relevance of this water depth range for hydraulic heavy rainfall simulations should not be underestimated, as very shallow water depths are becoming increasingly important in 2D-hydraulic modelling with high resolution terrain models (Rai et al., 2010). The choice of roughness leads to diverging water depth, flow velocities and thus different concentration times resulting in a temporal and quantitative diverging peak discharge (Sauer and Ortlepp, 2021; Sanz-Ramos et al., 2021). Our results show clear dependencies of the roughness coefficient with vegetation cover, plant type and rain intensity, which should be taken into account in hydraulic simulations to improve the quality of the results. This study therefore contributes to more robust calibrations in infiltration models, since the influence of roughness on the shape of the hydrograph can now be estimated with higher accuracy.

Overall, our study is in agreement with previous studies demonstrating the increasing or decreasing roughness with increasing water depth in laboratory and field experiments (Díaz, 2005; Fraga et al., 2013; Wu et al., 1999; LUBW, 2016; Graf and Chhun, 1976; Fu et al., 2019). A summary of these values is shown in Fig. 12.

For example, Wu et al. (1999) investigated the impact of roughness in dependence to water level using an artificial channel and horsehair mattresses representing the influence of a ground-near dense vegetation on surface runoff. Water-depth-dependent Manning curves were determined for different vegetation heights. With fully submerged vegetation, the roughness coefficient tends to increase at low depths, but then decreases to an asymptotic constant, as the water level continues to rise. Since the mattresses are equivalent to a dense vegetation coverage, they correspond well to the results of the present study.

Díaz (2005) combined laboratory and field experiments, investigating the influence of different vegetation types on roughness. For grassland, similar values were determined as in Wu et al. (1999). Fraga et al. (2013) conducted rainfall runoff experiments on concrete and grass surfaces and tried to predict the rising and falling limb of the observed hydrograph with a numerical model solving the unsteady shallow water equations. Compared to the other studies shown, a very low vegetation height (5 mm) was used, which leads to a more rapidly decreasing roughness. The results showed also a significant rise of roughness at very low water depths and an increasing surface resistance with higher rain intensities due to the raindrop impact. This correlates with our findings as we detected also a coherence of rain intensity and roughness (Fig. 11).

Several authors compared the roughness functions in dependency of the degree of submergence with a strong agreement between different experimental setups (Graf and Chhun, 1976; Wilson and Horritt, 2002; Fraga et al., 2013). But this comparison is not appropriate for our data, because flow depth in the used experimental setup did not submerge vegetation.

Fu et al. (2019) conducted laboratory experiments on an inclined flume and varied artificial vegetation cover from almost 0 to 30 %. Their research stated an increasing roughness with flow depth which is contrary to the other studies, but can be explained by the used vegetation as the density increases with flow depth. The great achievement of their work is the derived empirical formula (Eq. (18)) directly considering the influence of vegetation coverage.

The LUBW (2016), an environmental authority of the state of Baden-Wuerttemberg in Germany, published a range of minimum and maximum plausible depth-dependent roughness values for the application in

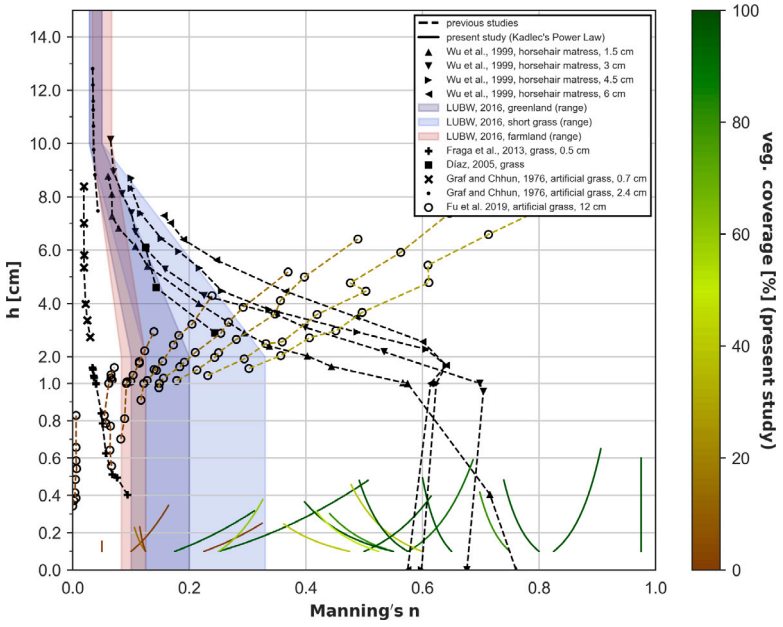

Fig. 12. Depth-dependent roughness relations from literature compared to the results achieved with Kadlec's Power Law. The label in the legend gives information about examined vegetation type and its height.

2D-hydraulic surface runoff modelling. For a water depth higher than 5 cm, they fit quite well to the other values presented, although the vegetation height was not considered. Comparing the given range of short grass and grassland to the present study, they highly underestimate the roughness for the near surface runoff.

We now provide robust values describing roughness for near surface runoff (<1 cm) for different types of vegetation and degree of vegetation coverage. The results give the hydraulic modeller an orientation, what range of roughness to choose for near surface runoff (Fig. 12). Furthermore, the knowledge gained about successive rain events can now help to better assess the influence of rainfall duration and intensity. For example, the roughness of very short and intense rain events would be underestimated with averaged values (Fig. 11).

5. Conclusions

Manning's n or a depth-dependent function of n is suitable to calculate the behaviour of surface runoff. A general valid roughness function should include the degree of vegetation coverage and the vegetation type.

Based on the main findings of our study, roughness values can be determined by measuring the outflow based on a comparably simple framework as. This renders the conduction of complex measurements of flow velocity and water level unnecessary.

The derived roughness values extend the current knowledge for shallow water depths. It is shown, that roughness has tended to be underestimated in some cases. For all examined sites, robust values could be derived, while surfaces with no vegetation or an extremely high vegetation density showed largest variability. For bare soil, this can be explained by rapid changes in the surface structure, potentially caused by crust formation and erosion. The variability of high density vegetation is assumed to be caused by plant type, as high vegetation coverage alone is not able to describe the differences between the sites.

This study contributes also to a more accurate calibration of infiltration models. Roughness has been estimated using the falling limb of the hydrograph when infiltration is nearly constant. Based on the identified roughness the impact of infiltration rate and roughness on the increasing segment of the hydrograph can be clearly separated. Consequently, it is possible to precisely calculate the change in infiltration rate for the entire artificial rainfall experiment.

Finally, the study shows clearly the possibilities and limitations of estimating roughness coefficients with data from artificial sprinkling experiments. The results of the study can be directly applied in hydraulic 2D modelling, as they give modellers an orientation for the selection of parameters, particularly, when low water depths are crucial for the generation of surface runoff, which is important for the simulation of heavy rainfall events.

CRediT authorship contribution statement

David Feldmann: Conceptualization, Methodology, Software, Visualization, Writing – original draft. **Patrick Laux:** Conceptualization, Writing – original draft, Supervision, Project administration, Fund acquisition. **Andreas Heckl:** Writing – review & editing. **Manfred Schindler:** Writing – review & editing. **Harald Kunstmann:** Writing – review & editing, Supervision.

Declaration of competing interest

The authors declare that they have no known competing financial interests or personal relationships that could have appeared to influence the work reported in this paper.

Data availability

The authors do not have permission to share data.

Acknowledgements

We highly acknowledge the data from artificial rainfall experiments provided by Ries et al. (2019). The raw data can be retrieved from https://doi.org/10.6094/UNIFR/151460. This work was funded by the BMBF, Germany research project KARE (grant number 01LR2006D). We thank the two anonymous reviewers for their fruitful comments, which helped to improve the quality of the manuscript.

References

Agassi, M., Benyamini, Y., Morin, J., Marish, S., Henkin, E., 1996. Runoff and erosion control in Israel. In: Runoff, Infiltration and Subsurface Flow of Water in Arid and Semi-Arid Regions, Vol. 21. Springer, Dordrecht, pp. 63–120. http://dx.doi.org/10.1007/978-94-017-2929-1_2.

Assouline, S., 2004. Rainfall-induced soil surface sealing: A critical review of observations, conceptual models, and solutions. Vadose Zone J. 3 (2), 570–591. http://dx.doi.org/10.2136/VZJ2004.0570.

Assouline, S., 2013. Infiltration into soils: Conceptual approaches and solutions. Water Resour. Res. 49 (4), 1755–1772. http://dx.doi.org/10.1002/wrcr.20155.

Barros, A.P., Colello, J.D., 2001. Surface roughness for shallow overland flow on crushed stone surfaces. J. Hydraul. Eng. 127 (1), 38–52. http://dx.doi.org/10.1061/(asce)0733-9429(2001)127:1(38).

Beven, K., 2004. Robert E. Horton's perceptual model of infiltration processes. Hydrol. Process. 18 (17), 3447–3460. http://dx.doi.org/10.1002/hyp.5740.

Bresson, L.M., Boiffin, J., 1990. Morphological characterization of soil crust development stages on an experimental field. Geoderma (Neth.) 47 (3), 301–325. http://dx.doi.org/10.1016/0016-7061(90)90035-8.

Bulti, D.T., Abebe, B.G., 2020. A review of flood modeling methods for urban pluvial flood application. Model. Earth Syst. Environ. 6 (3), 1293–1302. http://dx.doi.org/10.1007/s40808-020-00803-z.

Cantisani, A., Giosa, L., Mancusi, L., Sole, A., 2014. FLORA-2D : A new model to simulate the inundation in areas covered by flexible and rigid vegetation. Int. J. Eng. Innov. Technol. (IJEIT) 3 (8), 179–186.

Chow, V.T., 1959. Open Channel Hydraulics. McGraw-Hill, New-York.

David, A., Schmalz, B., 2020. Flood hazard analysis in small catchments: Comparison of hydrological and hydrodynamic approaches by the use of direct rainfall. J. Flood Risk Manag. 13:e12639 (4), http://dx.doi.org/10.1111/JFR3.12639.

Díaz, R.G., 2005. Analysis of Manning coefficient for small-depth flows on vegetated beds. Hydrol. Process. 19 (16), 3221–3233. http://dx.doi.org/10.1002/hyp.5820.

Ding, L., Fu, S., Zhao, H., 2021. Hydraulic properties affected by litter and stem cover under overland flow. Hydrol. Process. 35 (3), http://dx.doi.org/10.1002/hyp.14088.

Ding, Y., Jia, Y., Wang, S.S.Y., 2004. Identification of manning's roughness coefficients in shallow water flows. J. Hydraul. Eng. 130 (6), 501–510. http://dx.doi.org/10.1061/(ASCE)0733-9429(2004)130:6(501).

Emmett, W.W., 1970. The hydraulics of overland flow on hillslopes, Vol. 662-A. U.S. Geological Survey Professional Paper, http://dx.doi.org/10.3133/PP662A.

Engman, E.T., 1986. Roughness coefficients for routing surface runoff. J. Irrig. Drain. Eng. 112 (1), 39–53. http://dx.doi.org/10.1061/(asce)0733-9437(1986)112:1(39).

Esen, I., 1987. Least-squares estimates of the Horton infiltration parameters. Soil Sci. 144 (1), 6–10.

Farres, P., 1978. The role of time and aggregate size in the crusting process. Earth Surf. Process. 3 (3), 243–254. http://dx.doi.org/10.1002/ESP.3290030304.

Fernández-Pato, J., Caviedes-Voullième, D., García-Navarro, P., 2016. Rainfall/runoff simulation with 2D full shallow water equations: Sensitivity analysis and calibration of infiltration parameters. J. Hydrol. 536, 496–513. http://dx.doi.org/10.1016/j.jhydrol.2016.03.021.

Fraga, I., Cea, L., Puertas, J., 2013. Experimental study of the water depth and rainfall intensity effects on the bed roughness coefficient used in distributed urban drainage models. J. Hydrol. 505, 266–275. http://dx.doi.org/10.1016/j.jhydrol.2013.10.005.

Fu, S., Mu, H., Liu, B., Yu, X., Liu, Y., 2019. Effect of plant basal cover on velocity of shallow overland flow. J. Hydrol. 577, 123947. http://dx.doi.org/10.1016/J.JHYDROL.2019.123947.

Gaur, M.L., Mathur, B.S., 2003. Modeling event-based temporal variability of flow resistance coefficient. J. Hydrol. Eng. 8 (5), 266–277. http://dx.doi.org/10.1061/(asce)1084-0699(2003)8:5(266).

Graf, W.H., Chhun, V.H., 1976. Manning's roughness for artificial grasses. J. Irrigation Drain. Div. 102 (4), 413–423. http://dx.doi.org/10.1061/JRCEA4.0001116.

Horritt, M.S., Bates, P.D., Mattinson, M.J., 2006. Effects of mesh resolution and topographic representation in 2D finite volume models of shallow water fluvial flow. J. Hydrol. 329 (1–2), 306–314. http://dx.doi.org/10.1016/J.JHYDROL.2006.02.016.

Horton, R.E., 1933. The Role of infiltration in the hydrologic cycle. Trans. Am. Geophys. Union 14 (1), 446–460. http://dx.doi.org/10.1029/TR014i001p00446.

Huang, C.-h., Bradford, J., 1992. Applications of a laser scanner to quantify soil microtopography. Soil Sci. Am. J. 56 (1), 14–21. http://dx.doi.org/10.2136/sssaj1992.03615995005600010002x.

Hydrotec, 2022. HYDRO_AS-2D - 2D-flow model for water management applications - Reference Manual.

Jain, M.K., Kothyari, U.C., Ranga Raju, K.G., 2004. A GIS based distributed rainfall–runoff model. J. Hydrol. 299 (1–2), 107–135. http://dx.doi.org/10.1016/J.JHYDROL.2004.04.024.

Jarrett, R.D., 1990. Hydrologic and hydraulic research in mountain rivers. J. Am. Water Resour. Assoc. 26 (3), 419–429. http://dx.doi.org/10.1111/J.1752-1688.1990.TB01381.X.

Kadlec, R.H., 1990. Overland flow in wetlands: Vegetation resistance. J. Hydraul. Eng. 116 (5), 691–706. http://dx.doi.org/10.1061/(ASCE)0733-9429(1990)116:5(691).

Kaiser, M., Borga, M., Disse, M., 2020. Occurrence and characteristics of flash floods in bavaria (Germany). In: Climate Change Management. pp. 293–310. http://dx.doi.org/10.1007/978-3-030-37425-9{_}16.

Katz, D.M., Watts, F.J., Burroughs, E.R., 1995. Effects of surface roughness and rainfall impact on overland flow. J. Hydraul. Eng. 121 (7), 546–553. http://dx.doi.org/10.1061/(ASCE)0733-9429(1995)121:7(546).

Kim, J., Ivanov, V.Y., Katopodes, N.D., 2012. Hydraulic resistance to overland flow on surfaces with partially submerged vegetation. Water Resour. Res. 48 (10), W10540. http://dx.doi.org/10.1029/2012WR012047.

Lane, S.N., 2005. Roughness – time for a re-evaluation? Earth Surf. Process. Landf. 30 (2), 251–253. http://dx.doi.org/10.1002/ESP.1208.

Lawrence, D.S., 2000. Hydraulic resistance in overland flow during partial and marginal surface inundation: Experimental observations and modeling. Water Resour. Res. 36 (8), 2381–2393. http://dx.doi.org/10.1029/2000WR900095.

LUBW, 2016. Leitfaden Kommunales Starkregenrisikomanagement in Baden-Württemberg. LUBW Landesanstalt für Umwelt Messungen und Naturschutz Baden-Württemberg, Karlsruhe.

Manning, R., 1891. On the flow of water in open channels and pipes. Trans. Inst. Civ. Eng. Irel. 20, 161–207.

McIntyre, D.S., 1958. Permeability measurements of soil crusts formed by raindrop impact. Soil Sci. 85 (4), 185–189.

Moré, J., Garbow, B., Hillstrom, K., 1980. User guide for MINPACK-1. [In FORTRAN]. Technical Report, Argonne National Laboratory (ANL), Argonne, IL (United States), http://dx.doi.org/10.2172/6997568.

Mügler, C., Planchon, O., Patin, J., Weill, S., Silvera, N., Richard, P., Mouche, E., 2011. Comparison of roughness models to simulate overland flow and tracer transport experiments under simulated rainfall at plot scale. J. Hydrol. 402 (1–2), 25–40. http://dx.doi.org/10.1016/j.jhydrol.2011.02.032.

Özgen, I., Teuber, K., Simons, F., Liang, D., Hinkelmann, R., 2015. Upscaling the shallow water model with a novel roughness formulation. Environ. Earth Sci. 74 (11), 7371–7386. http://dx.doi.org/10.1007/S12665-015-4726-7.

Pironneau, O., 1988. Finite Element Methods for Fluids. Wiley, Paris.

Rai, R.K., Upadhyay, A., Singh, V.P., 2010. Effect of variable roughness on runoff. J. Hydrol. 382 (1–4), 115–127. http://dx.doi.org/10.1016/j.jhydrol.2009.12.022.

Ribolzi, O., Patin, J., Bresson, L.M., Latsachack, K.O., Mouche, E., Sengtaheuanghoung, O., Silvera, N., Thiébaux, J.P., Valentin, C., 2011. Impact of slope gradient on soil surface features and infiltration on steep slopes in northern laos. Geomorphology 127 (1–2), 53–63. http://dx.doi.org/10.1016/J.GEOMORPH.2010.12.004.

Ries, F., Kirn, L., Weiler, M., 2019. Runoff response from extreme rainfall events on natural hillslopes: A data set from 132 large-scale sprinkling experiments in south-western Germany. 2. Version. http://dx.doi.org/10.6094/UNIFR/151460.

Ries, F., Kirn, L., Weiler, M., 2020. Runoff reaction from extreme rainfall events on natural hillslopes: A data set from 132 large-scale sprinkling experiments in south-western Germany. Earth Syst. Sci. Data 12 (1), 245–255. http://dx.doi.org/10.5194/essd-12-245-2020.

Romkens, M.J., Wang, J.Y., 1986. Effect of tillage on surface runoff. Trans. Am. Soc. Agric. Eng. 29 (2), 429–433. http://dx.doi.org/10.13031/2013.30167.

Sañudo, E., Cea, L., Puertas, J., 2020. Modelling pluvial flooding in urban areas coupling the models iber and SWMM. Water 12 (9), 2647. http://dx.doi.org/10.3390/w12092647.

Sanz-Ramos, M., Bladé, E., González-Escalona, F., Olivares, G., Aragón-Hernández, J.L., 2021. Interpreting the manning roughness coefficient in overland flow simulations with coupled hydrological-hydraulic distributed models. Water (Switzerland) 13 (23), 3433. http://dx.doi.org/10.3390/w13233433.

Sauer, A., Ortlepp, R., 2021. Parameter uncertainties in flood hazard analysis of heavy rain events. ASCE-ASME J. Risk Uncertain. Eng. Syst. A 7 (2), http://dx.doi.org/10.1061/AJRUA6.0001125.

Savant, G., Trahan, C.J., Pettey, L., McAlpin, T.O., Bell, G.L., McKnight, C.J., 2019. Urban and overland flow modeling with dynamic adaptive mesh and implicit diffusive wave equation solver. J. Hydrol. 573, 13–30. http://dx.doi.org/10.1016/J.JHYDROL.2019.03.061.

Seibert, S.P., Auerswald, K., Fiener, P., Disse, M., Martin, W., Haider, J., Michael, A., Gerlinger, K., 2011. Surface runoff from arable land – a homogenized data base of 726 rainfall simulation experiments. Hydrol. Earth Syst. Sci. (Special issue), http://dx.doi.org/10.1594/GFZ.TR32.2.

Sepaskhah, A.R., Bondar, H., 2002. Estimation of manning roughness coefficient for bare and vegetated furrow irrigation. Biosyst. Eng. 82 (3), 351–357. http://dx.doi.org/10.1006/bioe.2002.0076.

Simons, F., Busse, T., Hou, J., Özgen, I., Hinkelmann, R., 2014. A model for overland flow and associated processes within the Hydroinformatics Modelling System. J. Hydroinform. 16 (2), 375–391. http://dx.doi.org/10.2166/HYDRO.2013.173.

Smith, M.W., 2014. Roughness in the earth sciences. Earth-Sci. Rev. 136, 202–225. http://dx.doi.org/10.1016/j.earscirev.2014.05.016.

Tatard, L., Planchon, O., Wainwright, J., Nord, G., Favis-Mortlock, D., Silvera, N., Ribolzi, O., Esteves, M., Huang, C.H., 2008. Measurement and modelling of high-resolution flow-velocity data under simulated rainfall on a low-slope sandy soil. J. Hydrol. 348 (1–2), 1–12. http://dx.doi.org/10.1016/j.jhydrol.2007.07.016.

Tsihrintzis, V.A., Wu, F.-C., Shen, H.W., Chou, Y.-J., 2001. Discussion and closure: Variation of roughness coefficients for unsubmerged and submerged vegetation. J. Hydraul. Eng. 127 (3), 241–245. http://dx.doi.org/10.1061/(ASCE)0733-9429(2001)127:3(241).

Wilson, C.A., Horritt, M.S., 2002. Measuring the flow resistance of submerged grass. Hydrol. Process. 16 (13), 2589–2598. http://dx.doi.org/10.1002/HYP.1049.

Wu, F.-s., 2008. Characteristics of flow resistance in open channels with non-submerged rigid vegetation. J. Hydrodyn. 20 (2), 239–245. http://dx.doi.org/10.1016/S1001-6058(08)60052-9.

Wu, F.-C., Shen, H.W., Chou, Y.-J., 1999. Variation of roughness coefficients for unsubmerged and submerged vegetation. J. Hydraul. Eng. 125 (9), 934–942. http://dx.doi.org/10.1061/(ASCE)0733-9429(1999)125:9(934).

Zhang, W., Cundy, T.W., 1989. Modeling of two-dimensional overland flow. Water Resour. Res. 25 (9), 2019–2035. http://dx.doi.org/10.1029/WR025I009P02019.

Zhang, J., Zhang, S., Chen, S., Liu, M., Xu, X., Zhou, J., Wang, W., Ma, L., Wang, C., 2021. Overland flow resistance law under sparse stem vegetation coverage. Water (Switzerland) 13 (12), 1657. http://dx.doi.org/10.3390/w13121657.